PNL-SA--19687

DE92 004486

Thermal Conductivities of Thin, Sputtered Optical Films

C. H. Henager, Jr.
W. T. Pawlewicz

May 1991

Work Supported by
the U.S. Department of Energy
under Contract DE-AC06-76RLO 1830

Pacific Northwest Laboratory
Richland, Washington 99352

DISCLAIMER

Thermal Conductivities of Thin, Sputtered Optical Films

C.H. Henager, Jr. and W.T. Pawlewicz*

Pacific Northwest Laboratory

Richland, WA 99352

The normal component of the thin film thermal conductivity has been measured for the first time for several advanced sputtered optical materials. Included are data for single layers of boron nitride (BN), aluminum nitride (AlN), silicon aluminum nitride (Si-Al-N), silicon aluminum oxynitride (Si-Al-O-N), silicon carbide (SiC), and for dielectric-enhanced metal reflectors of the form $Al(SiO_2/Si_3N_4)^n$ and $Al(Al_2O_3/AlN)^n$. Sputtered films of more conventional materials like SiO_2, Al_2O_3, Ta_2O_5, Ti, and Si have also been measured. The data show that thin film thermal conductivities are typically 10 to 100 times lower than conductivities for the same materials in bulk form. Structural disorder in the amorphous or very fine-grained films appears to account for most of the conductivity difference. Conclusive evidence for a film/substrate interface contribution is presented.

Key Words: thermal conductivity, sputtered optical films, thermal comparator, dielectric-enhanced metal reflectors, structural disorder, film/substrate interface.

---

* now at Litton/Itek Optical Systems, Lexington, MA 02173

I. INTRODUCTION

A wide variety of dielectric and metal films are currently being examined for advanced optical elements where high power densities are encountered. Both high and low refractive index materials are necessary for building multi-layered dielectric stacks, and all materials are required to be thermally and environmentally stable. Oxides and nitrides have the necessary optical properties, are easily deposited as high quality films, and are very stable. High thermal conductivities are also required, since the ability of an optical element to dissipate heat is often a limiting factor in optical designs. Uncertainties in optical film thermal conductivities can impose limitations on design accuracy [1]. This is especially true since it is now accepted that thin dielectric films have thermal conductivities much lower than comparable bulk materials. This means that indiscriminate use of bulk conductivity data in optical element design and damage calculations is highly inaccurate.

A variety of measurement techniques has been utilized to make thin film thermal conductivity measurements, including thermal comparators [2-4], specialized film geometries (including measurements on free standing films) [5-8], laser calorimetry [9,10], and flash radiometry [11]. The use of specialized film geometries [7,12-14] offers the greatest potential to achieve an understanding of thin film thermal and electronic processes, but these methods are impractical for optical film development research. The thermal comparator technique allows standard film/substrate geometries to be used in a nondestructive manner and is rapid and easy to use. This technique was developed to measure thermal conductivities of bulk specimens [2], but has been adopted for thin film use [3,4]. Briefly, a heated probe is brought into contact with the film/substrate system mounted on a heat sink. A temperature difference develops between the probe tip and a probe reference heat reservoir. The difference is proportional to the conductivity of the film/substrate system: small for poor conductors and large for good conductors.

All of the above techniques have consistently indicated that thin film thermal conductivities, when measured parallel to the film growth direction, are much smaller than bulk values. Boiko et al. [5]

and Nath and Chopra [6] measured in-plane thermal conductivities of deposited metal films and found good agreement with bulk values for films thicker than about 5000 Å. This immediately suggests that there is a large thermal resistance at the film substrate interface. However, Decker et al. [8] observed low thermal conductivity of free standing SiO_2 films when measured parallel to the film growth direction, suggesting that structural disorder also plays a major role in determining thin film conductivities.

The majority of other studies have examined oxide films such as SiO_2 and Al_2O_3. Lambropoulos et al. [3] also measured flouride films. Ristau and Ebert [9] measured e-beam deposited films of Al_2O_3, TiO_2, HfO_2, Ta_2O_5, and SiO_2 on fused silica substrates and found that only Al_2O_3 had a value close to the bulk. The other films had from one to several orders of magnitude lower thermal conductivities than bulk values. Lambropoulos et al. [3] observed large differences between thin films and bulk materials such as TiO_2, Al_2O_3, and MgF_2. Ogden et al. [4] observed that thick (up to 85 μm) films of anodized aluminum coatings, nominally Al_2O_3, had average thermal conductivities of 0.73 W/mK compared to 30 W/mK for bulk, polycrystalline Al_2O_3.

The silica glass system has been studied extensively by these thin film techniques; measured thin film thermal conductivities are found to be from a factor of two to an order of magnitude smaller than bulk conductivities. Decker et al. [8] measured SiO_2 films between 0.5 and 1 μm thick and found values an order of magnitude lower than in bulk SiO_2, 0.17 to 0.28 W/mK compared to 1.4 W/mK for bulk fused silica [15]. Ristau and Ebert [9] measured thin film values of 0.1 W/mK for 1 μm thick SiO_2 films. Lambropoulos et al. [3] report values of 0.45 to 0.61 W/mK for e-beam evaporated SiO_2 and 0.41 to 1.05 W/mK for ion beam sputtered SiO_2. Swartz and Pohl [7] observe thin film conductivities approximately a factor of two smaller than bulk SiO_2. The work of Swartz and Pohl [7] suggests that the film/substrate interface, or near-interface region, contributes to phonon scattering sufficient to account for these differences. This additional scattering is proposed to come from local structural disorder [7].

II. EXPERIMENTAL PROCEDURES

A. Thermal Comparator Technique

A thermal comparator was built at PNL and used to obtain thermal conductivities using an approximate analytical expression (Appendix). The comparator consists of a copper probe with a fine tip ($r_p \sim 0.2$ mm) machined on the end, a large copper plate heat sink (15 cm diameter x 2.5 cm thick), and a Plexiglass enclosure (Figure 1). The probe is mounted on a stem attached to an x-y-z manipulator, which allows accurate positioning of the probe tip on the specimen. A constantan wire is placed down the stem through a hole drilled in the probe and makes a soldered copper-constantan (Type T) thermocouple junction at the probe tip. Small weights are placed on the probe assembly to give a total probe mass of about 200 g. A reference thermocouple is placed in the probe body and a thermocouple is placed in the copper heat sink. The probe is heated to about 85 C using a small heater wrapped around the probe body and the temperature is controlled to ±0.5 C using a standard three mode controller operating a 200 W power supply. The specimens are placed on the copper heat sink held at ambient temperature on a small steel table on which a connector strip is attached for the various electrical connections. The Plexiglass enclosure shelters the comparator from laboratory breezes. An HP 85 computer with an HP data acquisition box was used to acquire the comparator data, which consists of the probe reference temperature, the temperature difference between the probe tip and probe body (reservoir) at contact, and the heat sink temperature. An operational amplifier with a gain of 10^4 was used to amplify the probe tip/probe body temperature difference signal, which typically ranged from 4 to 30 μVolts (45.7 μV/K for Cu-Cn Type T thermocouple).

As a check of the comparator, several bulk standards were measured to demonstrate the square root dependence of the change in temperature between the probe tip and reservoir as a function of thermal conductivity observed by Powell [2] (Figure 2). Figure 2 illustrates how the comparator

can be used as a calibration curve to determine the thermal conductivity of an unknown bulk material in a "comparative" manner.

Use of the comparator with thin film specimens required the development of an experimental technique and analysis method distinct from that used to measure bulk conductivities. Measurements of coated substrates indicated a large reduction in thermal conductivity from the uncoated substrates, which for the experiments reported here was polished single crystal silicon. This reduction in conductivity was used to extract that portion of the thermal resistance due to the coating (film) but can only be used to give the effective conductivity of the film plus film/substrate interface system (see Appendix). The analysis method requires that films of several different thicknesses be deposited and measured to determine the film conductivity.

A probe temperature of 85 C and a heat sink temperature of 22 C (ambient) were chosen to give a large temperature difference signal without heating the heat sink. Typically, the heat sink temperature would rise about 1 C during a several-hour data acquisition session. The probe mass of 200 g was chosen by trial and error to give a reproducible probe tip/specimen contact. As with other thermal comparators, when the probe tip makes contact with the specimen a temperature difference is established between the probe tip and the probe body (reservoir) as heat flows from the probe into the specimen. For the PNL thermal comparator, a steady-state temperature difference was established within 2 sec after contact. The computer data acquisition system was programmed to discard temperature data acquired before this steady state temperature was reached. Average temperature differences were computed using probe reference temperatures acquired several seconds before and after probe tip contact was made. Contact was made for 5 sec, with the first 2 sec of data discarded as discussed above. Typically 7 to 10 contacts were made for a given film thickness to obtain a single data point. Since the probe tip/film contact resistance was of concern during this measurement, a high thermal conductivity grease was applied to the probe tip to ensure uniform contact between the probe tip and specimen. All 7 to 10 contacts for a given data point

were made at the same location using the same thermal grease spot. New grease was applied to the probe tip on shifting the measurement to a new location or new specimen.

B. Sputtered Optical Films

A wide variety of films (Table 1) were deposited on (111) single-crystal, highly polished (5 Å rms) Si substrates (3.8 cm diameter x 0.64 cm thick), a standard substrate used in optical film research at PNL. When possible, several film thicknesses were chosen to give a range spanning the thickness of interest. For example, typical single layer dielectric film thicknesses for optical applications range from 0.5 μm to 2 μm, while multilayered stacks range from 1 to 5 μm. The Si-Al-N and Si-Al-O-N films were quite thick and ranged from 10 to 60 μm in thickness. A limited amount of data was obtained from films of only a single thickness using a bare Si substrate as a zero thickness film.

Films were sputtered using a variety of techniques, which included RF diode reactive sputtering from 15 cm targets and both large chamber (2 meter substrates) and small chamber (35 cm substrates) magnetron sputtering [17,18]. No evaporated films were measured. Each of the sputtering chambers was outfitted with specimen holders to allow the use of the standard 3.8 cm Si substrates.

C. Method of Analysis of Thin Film Data and Principal Measurement Uncertainties

An analysis of the series of thermal resistances involved in the comparator measurement is shown in the appendix and an approximate expression for the film thermal conductivity is obtained as (equation 1 and A14)

$$K_3 = k^f_{th} = \frac{\Delta K_1 r_1}{m A_3} \qquad (1)$$

where k^f_{th} is the film thermal conductivity (including the film/substrate interface), K_1 is the thermal conductivity of the probe body and is equal to that of copper, 401 W/mK, r_1 is the probe tip radius and is set equal to r^{eff}_p, m is the slope of a fitted line for the temperature ratio (equation A10) as a function of film thickness, and A_3 is the probe tip/specimen contact area, $\pi r^{eff}_p{}^2$. Making these substitutions then gives

$$k^f_{th}\left(\frac{W}{m\,K}\right) = \frac{1.608 \times 10^5 \left(\frac{W}{m\,K}\right)}{\pi\, r^{eff}_p(m)\; m\left(\mu m^{-1}\right) 10^6} \qquad (2)$$

where r^{eff}_p is 1.5×10^{-4} m as determined from micrographs of probe tip contact imprint areas from actual measurement spots using the thermal grease (Figure 3) and m is determined using a least squares fitted line to the temperature ratio vs film thickness data. The temperature ratio is given by $(T_p - T_b)/(T_p - T_t)$, where T_p is the probe reference temperature, T_b is the heat sink temperature, and T_t is the probe tip temperature after the steady state contact temperature is established.

The largest experimental uncertainties are the determination of r^{eff}_p and the assumption that it remains relatively constant from specimen to specimen. Underlying this are the assumptions, discussed in the appendix, that lateral heat flow in the films can be neglected and that the actual probe tip/specimen contact area can be used for r^{eff}_p. Obviously, the former assumption is best for low conductivity films. The uncertainty in r^{eff}_p is estimated to be ±50%. Measured thermal conductivities have the same uncertainty.

Statistical tests suggest that there is also a measurement uncertainty related to lack of repeatability in probe tip placement from data set to data set for the same specimens, though not within a given data set. Typical standard deviations from the mean for a given data set (repeated contacts on the same thermal grease spot) are less than 5% and often less than 2%, which is excellent reproducibility. However, statistical t-tests occasionally indicate that separate data sets do not satisfy the hypothesis that 1) a given data set belongs to the parent population (using a one-sample,

two-tailed t-test at the 95% confidence level as shown in Figure 4) or 2) two data sets belong to the same population (using an unpaired, two-tailed t-test at the 95% confidence level as shown in Figure 5). These statistical t-tests suggest a systematic error in the measurement technique, most likely the probe tip contacting the specimen at a slight angle or with a different part of the probe tip than in the other data set. Still, it is concluded that the thermal comparator technique developed here provides data of useful accuracy where none existed previously.

III. RESULTS AND DISCUSSION

Measured thin film thermal conductivities are shown (Table 1, Figure 6) for a wide variety of dielectric and metal films and for two multi-layered stacks. For many of the materials, these are the first measurements ever reported. The sputtered Ti and Si films were studied for calibration purposes and to explore differences between a metal film (electron dominated heat conduction) and a dielectric (phonon dominated heat conduction). Ti was chosen because it is a poor thermal conductor for a metal and because reasonable signal levels (temperature differences) could be expected for Ti films in the micron thickness range.

First examination of Table 1 reveals a large discrepancy between measured thin film thermal conductivities and handbook bulk values. This comparisons is, of course, not meaningful without an appreciation of the structural differences between the films and the bulk materials in the handbooks. Thin dielectric films are typically amorphous (glassy) or microcrystalline, resulting in reduced thermal conductivity due to increased phonon scattering from lattice imperfections. However, a more complete explanation is needed since the structure of sputtered SiO_2 is not appreciably different from that of bulk glasses and yet the measured thermal conductivity of SiO_2 films is an order of magnitude lower than handbook bulk values. In particular, the interface between the film and the substrate must be considered as a barrier to phonon transport (barrier to heat transfer) [7]. Studies of these interfaces, where the films nucleate and grow from the vapor,

supports this idea since structural disorder, in the form of lattice strain and growth defects, tends to be concentrated there [7,12,13,16,19].

Therefore, the two leading mechanisms for the reduced thermal conductivities of sputtered thin films are 1) structural disorder within the film and 2) a barrier to heat transfer at the film/substrate interface. As will be discussed below, it is difficult at the present time to distinguish between these mechanisms, both of which play important roles. The barrier that is postulated to exist at the film/substrate interface may actually be local structural disorder at the film/substrate near-interface region, and may extend only a few Angstroms within the film [7,12,13]. The thermal comparator technique gives a measure of the thermal response of the film/substrate system as a whole and cannot separate distinct components. However, comparison of thin film thermal conductivities of both phonon-dominated and electron-dominated thermal conductors do indicate that, although the film/substrate interface is a common denominator for all the films tested, it appears to be more significant for dielectric films where the heat conduction is phonon-dominated.

Table 1. Summary of Thin Film Thermal Conductivity Measurements

Material	Film Structure	Thermal Conductivity (W/mK) PNL Data Thin Film	Other Data Thin Film	Bulk Conductivity	Ratio
		Thermal Conductivity (W/mK)			
Ti	(001) texture 200 Å grains	1.6-2.0		21.9	11-14
Si	(111) texture 300 Å grains	1.0		148	148
SiO_2 [17]	glassy	0.12	0.1 [10] 0.17 to 0.28 [8] 0.41 to 1.05 [3]	1.3	11
Al_2O_3 [17]	glassy	0.12	0.25 [8] 0.72 [3] 0.73 [4]	28	233
Ta_2O_5 [17]	glassy	0.12			
BN [17]	glassy	0.32		62 (a axis) 1.5-2.9	194 4.7-9.1
Si_3N_4 [17]	glassy	0.15		10	67
SiC [17]	glassy	0.12		25	208
$Si_{.7}Al_{.3}N$ [20]	(111) texture microcrystalline	0.82			
$Si_{.6}Al_{.4}N$ [20]	(111) texture microcrystalline	0.88			
$Si_{.6}Al_{.4}NO$ [20] N:O = 2:1	(111) texture microcrystalline	0.83			
$Si_{.6}Al_{.4}NO$ [20] N:O = 1:2	(111) texture microcrystalline	0.62			
$Al(SiO_2/Si_3N_4)^n$ [17]	glassy	0.25			
$Al(Al_2O_3/AlN)^n$ [17]	glassy	0.32			

A. Sputtered Ti and Si Films

Thin sputtered films of Ti (Ti#1: 1.7, 4.2, and 8.5 μm thick; and Ti#2: 1.15, 2.8, and 5.7 μm thick) and Si (2.0, 4.9, and 9.9 μm thick) were sputtered onto Si substrates in a quadrant arrangement such that one Si substrate contained three quadrants of sputtered film, one of each of the above thicknesses, and one bare quadrant. Sputtering was performed using small (5 cm) magnetron sources operating at 420 VDC and 2 A at a pressure of 2.2 mTorr Ar. Sputtering rates were 570 Å/min for Ti#1, 380 Å/min for Ti#2, and 667 Å/min for Si using sputtering times of 30, 75, and 150 minutes for each quadrant, respectively. A Sloan M-200 Angstrometer using Na vapor illumination was used to measure the film thickness of the thinnest quadrant and to obtain the other quadrant thicknesses by assuming similar sputtering rates. XRD indicated that the Ti films were (001) oriented with a 200 ± 20 Å grain size and the Si films were (111) oriented with a 300 ± 30 Å grain size.

Each quadrant was measured using the thermal comparator technique and the thin film thermal conductivities were determined (Figure 7). The value of k^f_{th} for sputtered Ti (2.0 W/mK) is 11 times smaller than that for bulk Ti (21.9 W/mK), while that for sputtered Si (0.97 W/mK) is 150 times smaller than bulk polycrystalline Si (148 W/mK). Additionally, four point probe in-plane electrical conductivity measurements of sputtered Ti gave an average value of $\sigma^f_{Ti} = 1.6 \times 10^4$ $(\Omega cm)^{-1}$, which is 68% of the measured bulk value of $\sigma_{Ti} = 2.34 \times 10^4$ $(\Omega cm)^{-1}$. No electrical measurements were made for the Si films.

The measured reduction in electrical conductivity is consistent with the observed fine grain sized Ti structure, with a grain size of 200 ± 20 Å calculated from XRD peak broadening. Additional grain boundary scattering and the structural disorder associated with the columnar structure observed in sputtered metal films could easily account for this reduction. Grain boundaries and disorder would also be expected to reduce the measured thermal conductivity by this same factor in compliance with the Wiedemann-Franz law, which states that $\kappa/\sigma T$, the Lorenz number, is roughly constant

for metallic materials. For bulk Ti at 273 K the Lorenz number is 3.43×10^{-8} $W\Omega/K^2$. Sputtered Ti films should have a thermal conductivity roughly 0.68 times lower than the bulk, or about 15 W/cmK, whereas the measured value of 2 W/mK is 7.5 times smaller. Clearly, additional factors are acting to reduce the film thermal conductivity. Since the electrical conductivity was measured in-plane and the thermal conductivity was measured through the thickness and includes the film/substrate interface, it can be inferred that additional scattering centers are present at this interface that do not influence in-plane measurements.

Phonon heat conduction is expected to be more sensitive to scattering centers present at the film/substrate interface, perhaps due to a local increase in umklapp processes. This hypothesis is supported by the much greater decrease in thermal conductivity observed for the sputtered Si compared to the sputtered Ti (150 times smaller compared to 7.5 times smaller) for similar fine grain size and, presumably, similar microstructure. It is concluded, therefore, that for dielectric films, in which heat conduction is phonon-dominated, large heat transfer barriers will exist due to the presence of the film/substrate interface and that these barriers will dominate the measured thin film thermal conductivities. However, structural disorder in the film will also affect thermal conductivities.

B. Dielectric Films (Single Layer and Multi-Layered)

Measured thermal conductivities of dielectric films (Table 1, Figure 6) show a narrow range of values (0.12-0.88 W/mK) consistent with either an interface dominated heat transfer barrier or structural disorder. The relative constancy of these values is perhaps more fundamentally important than any relationship between thin film values and bulk values (Figure 8). As shown in Figure 8, the films are best distinguished by both their bulk and film structural characteristics. Comparisons between bulk and film conductivities are meaningless unless structural effects are taken into account. One cannot compare data for materials that are polycrystalline in bulk form but glassy as thin films with others that are both bulk glasses and thin film glasses. The different symbols in

Figure 8 are meant to aid in sorting out this variable and allowing valid comparisons to be made. In general, dielectric materials that are crystalline in bulk form but are glassy in thin film form have thin film conductivities that are in a narrow range from 0.12 to 0.32 W/mK even though their bulk conductivities range from about 2 to 62 W/mK. Not surprisingly, these materials also have the highest bulk/film conductivity ratios since both structural disorder and film/substrate interface effects are present in the thin films but not present in the bulk materials [7,12,13,16,19].

Structural effects can cause large differences in observed thin film conductivities, as can be seen by considering the data for SiO_2 [3,7-9] and the SiAlON materials [20]. Silica is the sole example here of a bulk glass material also having glassy thin films. Structural differences are minimized between bulk and film structures so that the decreased thin film conductivity is consistent with interface losses [7]. From the SiO_2 and the Ti data it can be inferred that the film/substrate interface accounts for about a 10- to 20-fold decrease in thermal conductivity from bulk materials. Therefore, additional reductions in thin film conductivities compared with bulk conductivities are most likely associated with structural differences in the body of the film, particularly for those materials that are bulk polycrystals but are glassy thin films. These bulk/film microstructural effects must contribute an additional order of magnitude decrease in measured conductivities (Table 1, Figure 6) to account for the BN, Si_3N_4, Al_2O_3, and SiC data. Structural effects are also apparent on examining the SiAlON data since these films were microcrystalline on the Si substrates and not glassy. The structure differences between the SiAlON films and the other dielectric films is due to good lattice matching between the SiAlON materials and the Si substrate and the fact the these depositions were performed at about 250 C [20]. Increased structural ordering probably accounts for the observed differences between the SiAlON films and the glassy dielectrics.

Compositional effects can also be observed in the data. Addition of AlN to Si_3N_4 to form a SiAlN material does increase thermal conductivity slightly, and addition of oxygen to SiAlN to form SiAlON materials does decrease thermal conductivity (Table 1, Figure 6). Both of these changes are consistent with simple rule of mixture calculations. For example, using bulk conductivity

values for Si_3N_4 (10 W/mK) and AlN (85 W/mK) a mixture of 60%Si_3N_4 and 40%AlN (corresponding to $Si_{.6}Al_{.4}N$) should have a conductivity of 40 W/mK, or roughly four times that of pure Si_3N_4. This is in good agreement with the measured ratio (1.5/8.8 = 5.9) for the thin films of Si_3N_4 and $Si_{.6}Al_{.4}N$. The additional conductivity gain can be considered to be due to reduction in structural disorder. Addition of AlN to the multi-layered stack coating system increases the thermal conductivity slightly, again consistent with rule of mixture arguments. However, these compositional effects are small relative to the roles played by structural disorder in the film and at the film/substrate interface.

The measured thermal conductivities of the two multi-layered dielectric stacks, $Al(SiO_2/Si_3N_4)^n$ (0.25 W/mK) and $Al(Al_2O_3/AlN)^n$ (0.32 W/mK), are more difficult to rationalize from the above arguments because these conductivities are larger than those measured for individual films of SiO_2, Si_3N_4, and AlN. The absence of detailed microstructural and interfacial structural data prevents a complete understanding. Perhaps the presence of the Al underlayer reduces the film/substrate interface effects. However, an obvious question is; why are there are not huge internal losses due to the series of film/film interfaces in these multi-layered stacks? One can only speculate that, since these individual layers are glassy in these multi-layered stacks (as observed in limited transmission electron microscopy examinations), interface losses at amorphous interfaces are very small compared to observed film/substrate losses. It is interesting to note that the dielectric stack containing AlN, $Al(Al_2O_3/AlN)^n$, possesses a higher thermal conductivity than the $Al(SiO_2/Si_3N_4)^n$ stack, which is consistent with the high conductivity of AlN compared to Si_3N_4.

IV. SUMMARY AND CONCLUSIONS

Measurement of the normal component of the thermal conductivity for an assembly of advanced and conventional single-layer and multi-layered sputtered optical materials shows that thin film thermal conductivities are usually 10 to 100 times lower than conductivities for the same materials in bulk form. In agreement with earlier measurements by other techniques for evaporated optical

films, these data clearly demonstrate the importance of using measured thin film conductivity values for optical system design calculations and performance estimates. The measured data also allow selection of the best materials for applications requiring high thermal conductivity and are expected to be of great utility to optical film designers, fabricators, and performance testers.

Structural disorder in the amorphous or fine-grained films appears to account for most of the conductivity difference. Structural disorder, for example, explains most of the orders of magnitude reduction in conductivity between amorphous Al_2O_3 and bulk crystalline sapphire, between Si and Ti films with 200-300 Å grain size and their single-crystalline counterparts, and between carbide and nitride films and bulk ceramic materials.

A film/substrate interfacial impedance is also apparent in the data, and must be accounted for in future thin film design and analysis. The interface barrier explains, for example, the difference in thermal conductivity for glassy SiO_2 films compared to bulk SiO_2 glass, and eliminates the apparent Wiedemann-Franz law violation for the in-plane electrical conductivity and the normal-component thermal conductivity in Ti films. The interface barrier appears to be much larger for dielectric phonon-transport materials than for metallic electron-transport materials. Such a barrier may consist of a region near the film/substrate interface of a high degree of disorder extending only a few phonon wavelengths into the film. This observation suggests that dielectric-enhanced metal reflectors are better choices than all-dielectric reflector designs for heat dissipation or cooling.

The first measured values of thermal conductivity are reported for single layers of advanced materials like BN, AlN, Si-Al-N, Si-Al-O-N, SiC, and for dielectric-enhanced metal reflectors of the form $Al(Al_2O_3/AlN)^n$ and $Al(SiO_2/Si_3N_4)^n$. The nitrides are seen to be better thermal conductors than the oxides in thin film form, just as they are in bulk form. These data will aid in development of high-thermal-conductivity materials and multi-layer structures. The single carbide examined (SiC) was found to be surprisingly low in thermal conductivity.

Rule of mixture calculations are found to be good predictors of thermal conductivity for more advanced and complex ternary nitride and oxynitride compositions and for multilayer optical stacks. Replacing Si_3N_4 with $Si_{.6}Al_{.4}N$, for example, increased measured conductivities somewhat more than the amount expected from the rule of mixtures, with an additional increase attributed to decreased structural disorder. These findings establish rule of mixture calculations as a new thermal design tool for future film development.

The PNL thermal comparator is shown to be a simple, inexpensive, rapid, and non-destructive technique to measuring the thermal performance of thin films in single or multilayer form.

APPENDIX

The following analysis was developed to extract thin film thermal conductivities from PNL's thermal conductivity apparatus. Figure A1 identifies the various components that make up the thin film thermal conductivity measurement. At each interface, heat flow is assumed to be proportional to the temperature difference and inversely proportional to the thermal resistance. Defining

$$T_i - T_j = \Delta T_{ij} = R_i Q \qquad \text{(A1)}$$

where ΔT_{ij} is the temperature difference between adjacent regions (numbered 1 to 5 in Figure A1), R_i is the thermal resistance of the ith interface, and Q is the steady state heat flow across the interfaces, conservation of energy requires that Q have the same value at each interface at steady state. As an example

$$T_1 - T_2 = \Delta T_{12} = R_1 Q \qquad \text{(A2)}$$

and R_1 is the thermal resistance to heat flow from the reservoir into the probe. The thermal resistance terms are conventionally written as a product of the thermal conductivity and geometrical factors as follows:

Probe Resistance (Region 1)

$1/R_1 = 4K_1r_1$ $\quad K_1$ = probe thermal conductivity

r_1 = probe tip radius

(This solution is for heat flow from a circular region into a semi-infinite cylinder and is from Carslaw, H.S., and J.C. Jaeger, Conduction of Heat in Solids, Oxford, N.Y., 1947, pp. 214-216)

Probe Tip/Film Resistance (Contact Resistance) (Region 2)

$1/R_2 = K_2A_2/t_2$ K_2 = contact conductivity

A_2 = contact area

t_2 = contact layer thickness

Film Resistance (Region 3)

$1/R_3 = K_3A_3/t_3$ K_3 = film conductivity

A_3 = contact area

t_3 = film thickness

(Here we assume there is no lateral heat flow in the film, which is a valid assumption if the film thermal conductivity is low and the film thickness is small compared to its radius)

Substrate Resistance (Region 4)

$1/R_4 = 4K_4r_4$ K_4 = substrate conductivity

r_4 = substrate radius

(Here we assume that heat flow from film into the substrate also obeys the semi-infinite solution discussed above)

Heat Sink Resistance (Region 5)

$R_5 \approx 0$ since $T_4 \approx T_5$ Assume $R_5 << R_1, R_2, R_3, R_4$

The resistances are considered to be in series such that

$$(T_1 - T_5) = \sum_{i}^{1-5} R_i Q = Q \sum_{i}^{1-5} R_i \tag{A3}$$

which can be solved for Q to give

$$Q = \frac{(T_1 - T_5)}{\sum_{i}^{1-5} R_i} \tag{A4}$$

Thus, we can write

$$T_1 - T_2 = R_1 Q = R_1 \frac{(T_1 - T_5)}{\sum_{i}^{1-5} R_i} \tag{A5}$$

which can be used to give

$$\frac{(T_1 - T_5)}{(T_1 - T_2)} = \frac{1}{R_1} \sum_{i}^{1-5} R_i = 1 + \frac{R_2}{R_1} + \frac{R_3}{R_1} + \frac{R_4}{R_1} + \frac{R_5}{R_1} \tag{A6}$$

Using the definitions for the R_i and neglecting R_5 gives

$$\frac{(T_1 - T_5)}{(T_1 - T_2)} = 1 + 4K_1 r_1 \left(\frac{t_2}{K_2 A_2}\right) + 4K_1 r_1 \left(\frac{t_3}{K_3 A_3}\right) + \frac{K_1 r_1}{K_4 r_4} \tag{A7}$$

Therefore, this gives

$$\frac{(T_1 - T_5)}{(T_1 - T_2)} = \left(\frac{4K_1 r_1}{K_3 A_3}\right) t_3 + \left[1 + \left(\frac{4K_1 r_1}{K_2 A_2}\right) t_2 + \frac{K_1 r_1}{K_4 r_4}\right] \tag{A8}$$

which is of the form for a line

$$y = mx + b \tag{A9}$$

where

$$y = \frac{(T_1 - T_5)}{(T_1 - T_2)} = \text{temperature ratio} \tag{A10}$$

$$x = t_3 = \text{film thickness} \tag{A11}$$

$$m = \frac{4K_1r_1}{K_3A_3} = \text{slope} \tag{A12}$$

$$b = \left[1 + \left(\frac{4K_1r_1}{K_2A_2}\right)t_2 + \frac{K_1r_1}{K_4r_4}\right] = \text{intercept} \tag{A13}$$

A plot of the temperature ratio as a function of film thickness is fit with a line using a least squares procedure. The resulting slope is used to solve for the film thermal conductivity, K_3, as

$$K_3 = k^f_{th} = \frac{4K_1r_1}{mA_3} \tag{A14}$$

where A_3 is the contact area between the probe tip and the film, r_1 is the probe tip radius, and K_1 is the thermal conductivity of the probe material. The contact area was determined by measuring the impression of the probe left on the film surface, the probe tip radius and probe thermal conductivity are known and, thus, the film conductivity can be calculated. Note that the probe contact resistance only appears in the intercept term and does not affect the measured value of the film thermal conductivity.

ACKNOWLEDGEMENTS

The authors would like to acknowledge the contribution of Bob Knoll and John Johnston to the design and construction of the thermal comparator, to Harold Kjarmo and Dave McCready for XRD, and to John Johnston, Don Stewart, and Mark Gross for thin film fabrication. Dick McCann contributed the analysis presented in the appendix. This work was partially supported by Rome Air Development Command under contract RADC F3 0602-90-F-0008.

REFERENCES

1. J.M. Halley and J.E. Midwinter, "Thermal Analysis of Optical Elements and Arrays on Thick Substrates with Convection Cooling," J. Appl. Phys., 62, 4055 (1987).

2. R.W. Powell, "Experiments Using a Simple Thermal Comparator for Measurement of Thermal Conductivity, Surface roughness and Thickness of Foils or of Surface Deposits," J. Sci. Instrum. 34, 485 (1957).

3. J.C. Lambropoulos, M.R. Jolly, C.A. Amsden, S.E. Gilman, M.J. Sinicropi, D. Diakomihalis, and S.D. Jacobs, "Thermal Conductivity of Dielectric Thin Films," J. Appl. Phys., 66, 4230 (1989).

4. T.R. Ogden, A.D. Rathsam, and J.T. Gilchrist, "Thermal Conductivity of Thick Anodic Oxide Coatings on Aluminum," Mater. Letters, 5, 84 (1987).

5. B.T. Boiko, A.T. Pugachev, and V.M. Bratsychin, "Method for the Determination of the Thermophysical Properties of Evaporated Thin Films," Thin Solid Films, 17, 157 (1973).

6. P. Nath and K.L. Chopra, "Experimental Determination of the Thermal Conductivity of Thin Films," Thin Solid Films, 18, 29 (1973).

7. E.T. Swartz and R.O. Pohl, "Thermal Resistance at Interfaces," Appl. Phys. Letters, 51, 2200 (1987).

8. D.L. Decker, L.G. Koshigoe, and E.J. Ashley, "Thermal Properties of Optical Thin Film Materials," in Laser Induced Damage in Optical Materials: 1984, NBS Special Publication 727, 291 (1984).

9. D. Ristau and T. Ebert, "Development of a Thermographic Laser Calorimeter," Appl. Optics, 25, 4571 (1986).

10. S.M.J. Akhtar, D. Ristau, and J. Ebert, "Thermal Conductivity of Dielectric Films and Correlation to Damage Threshold at 1064 nm," Laser Induced Damage in Optical Materials: 1986, NBS Special Publication 752, 345 (1986).

11. N. Tsutsumi and T. Kiyotsukuri, "Measurement of Thermal Diffusivity for Polymer Film by Flash Radiometry," Appl. Phys. Lett., 52, 442 (1988).

12. T. Klitsner and R.O. Pohl, "Phonon Scattering at a Crystal Surface from in situ-Deposited Thin Films," Phys. Rev. B, 34, 6045 (1986).

13. T. Klitsner and R.O. Pohl, "Phonon Scattering at Silicon Crystal Surfaces," Phys. Rev. B, 36, 6551 (1987).

14. D.G. Cahill and R.O. Pohl, "Thermal Conductivity of Amorphous Solids Above the Plateau," Phys. Rev. B, 35, 4067 (1987).

15. R.W. Powell and G.E. Childs, "Thermal Conductivity, " in American Institute of Physics Handbook, Third Edition, D.E. Gray, ed., McGraw-Hill, New York, pp. 4-142 to 4-162 (1972).

16. K.H. Guenther, "Microstructure of Vapor-Deposited Optical Coatings," Appl. Optics, 23, 3806 (1984).

17. W.T. Pawlewicz, D.C. Stewart, M.E. Gross, W.D. Bennett, and J.H. King, Surveillance Coatings Feasibility Evaluation, PNL-7433, TD2802 (1990).

18. W.T. Pawlewicz, D.C. Stewart, J.H. King, P.M. Martin, and W.D. Bennett, Large Diameter Reactively Sputtered Laser Optics: Low Temperature DC Magnetron Approach, RADC-TR-89-117 (1989).

19. J.M McCarthy, L.E. Thomas, W.T. Pawlewicz, W.S. Frydrych, and G.J. Exarhos, "Deposition of Dielectric Optical Coatings: A Microstructural Study of the Deposited Layers and Interfaces," in Proceedings of the Materials Research Society Meeting, San Diego, CA (1989).

20. R.W. Knoll and C.H. Henager, Jr., "Optical and Physical Properties of Sputtered SiAlON Films," submitted to J. Mater. Res. (1991).

Figure Captions

Figure 1. Photograph of PNL thermal comparator

Figure 2. Probe tip/probe body voltage difference as a function of $\sqrt{k_{th}}$ for various bulk standards.

Figure 3. Micrographs of a) Comparator probe tip and b) Probe tip imprint in thermal grease.

Figure 4. Comparison of the mean and standard deviations of 4 data sets taken from the same specimen, sputtered Si on Si, showing a low probability of set 4 belonging to the entire population.

Figure 5. Mean and standard deviation of two separate data sets for each of three specimens (three thicknesses) of sputtered Si_3N_4 on Si showing lack of correlation for the two sets taken on the thickest specimen, specimen 3. Other data sets are well correlated.

Figure 6. Measured thin film thermal conductivities of various sputtered optical films and multi-layered stacks.

Figure 7. Measured thermal conductivities of sputtered Ti and Si films (in W/mK).

Figure 8. Comparison of Handbook bulk thermal conductivities with measured thin film conductivities. Data segregated based on bulk and film structure, polycrystalline or glassy.

Figure A1. Schematic of probe tip region of thermal conductivity apparatus.

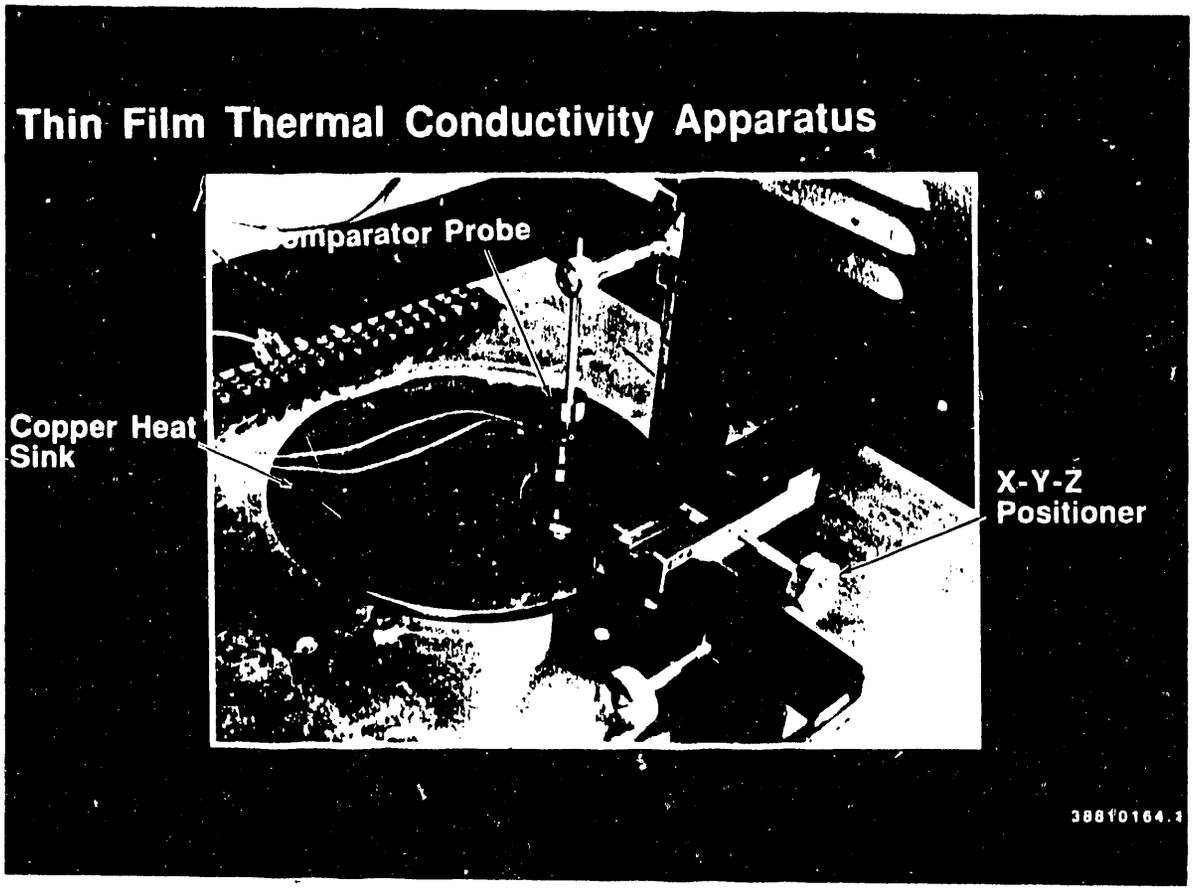

Figure 1. Photograph of PNL thermal comparator

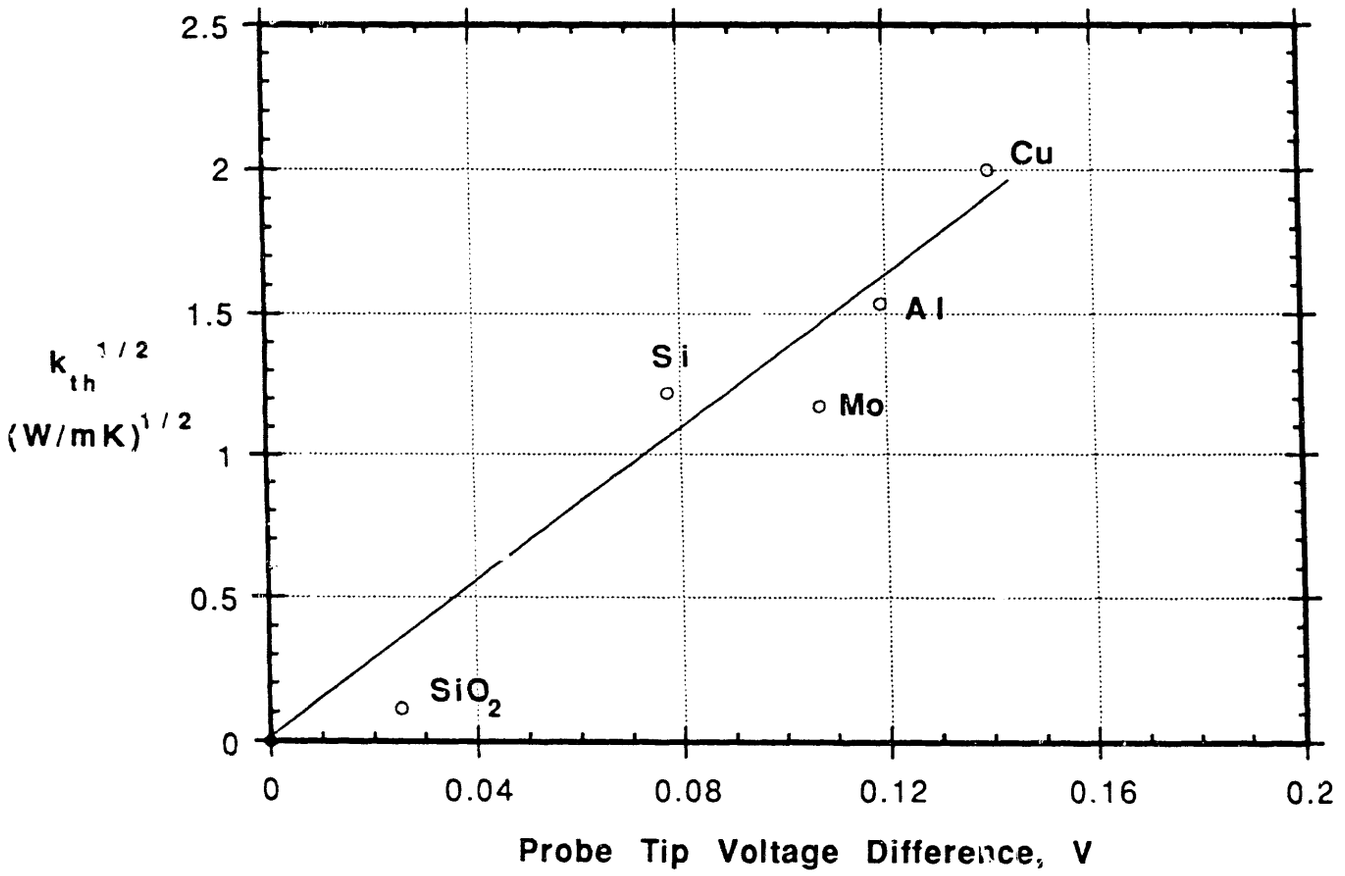

Figure 2. Probe tip/probe body voltage difference as a function of $\sqrt{k_{th}}$ for various bulk standards.

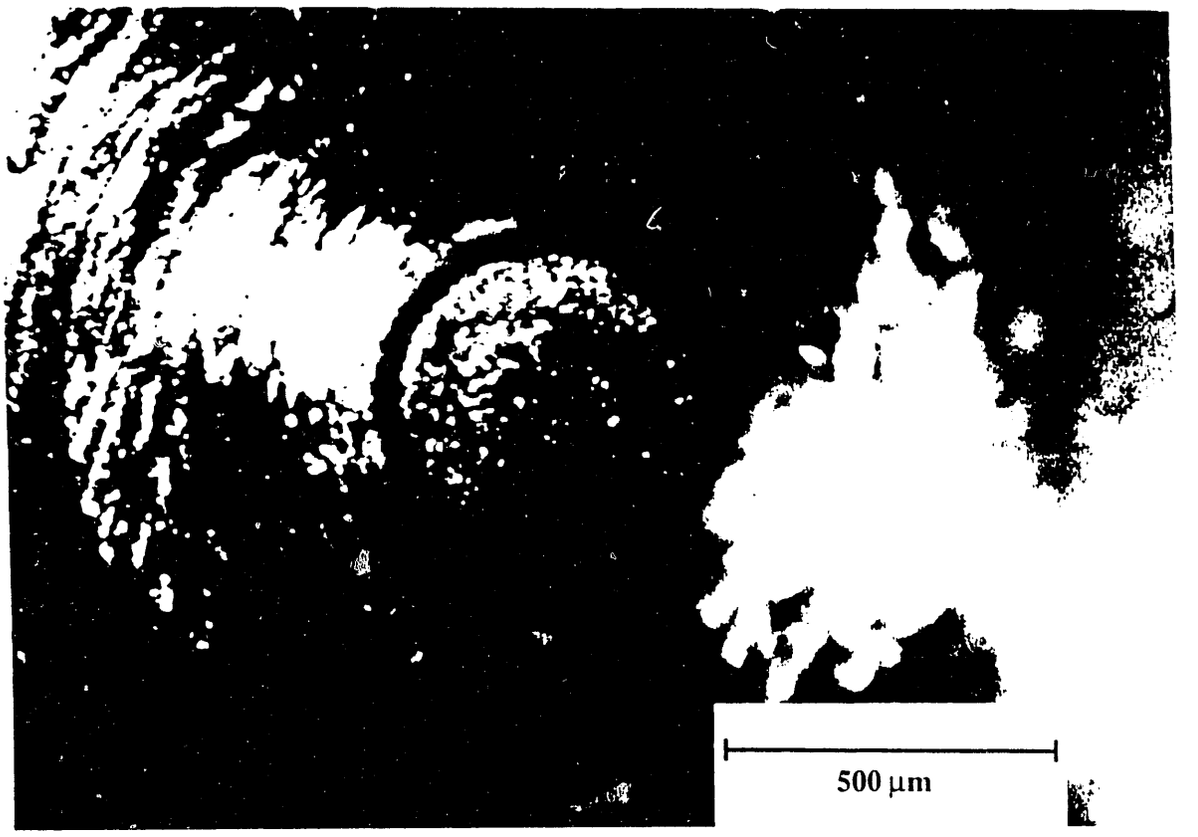

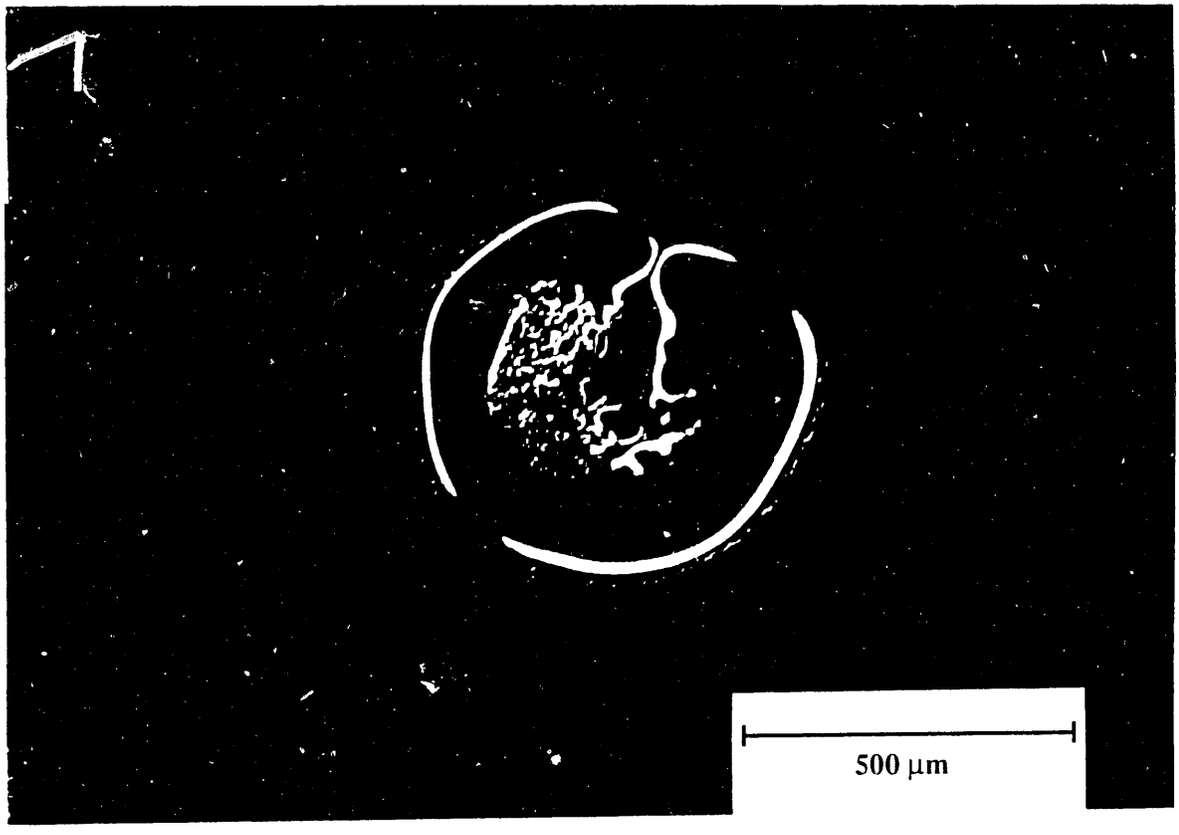

Figure 3. Micrographs of a) Comparator probe tip and b) Probe tip imprint in thermal grease.

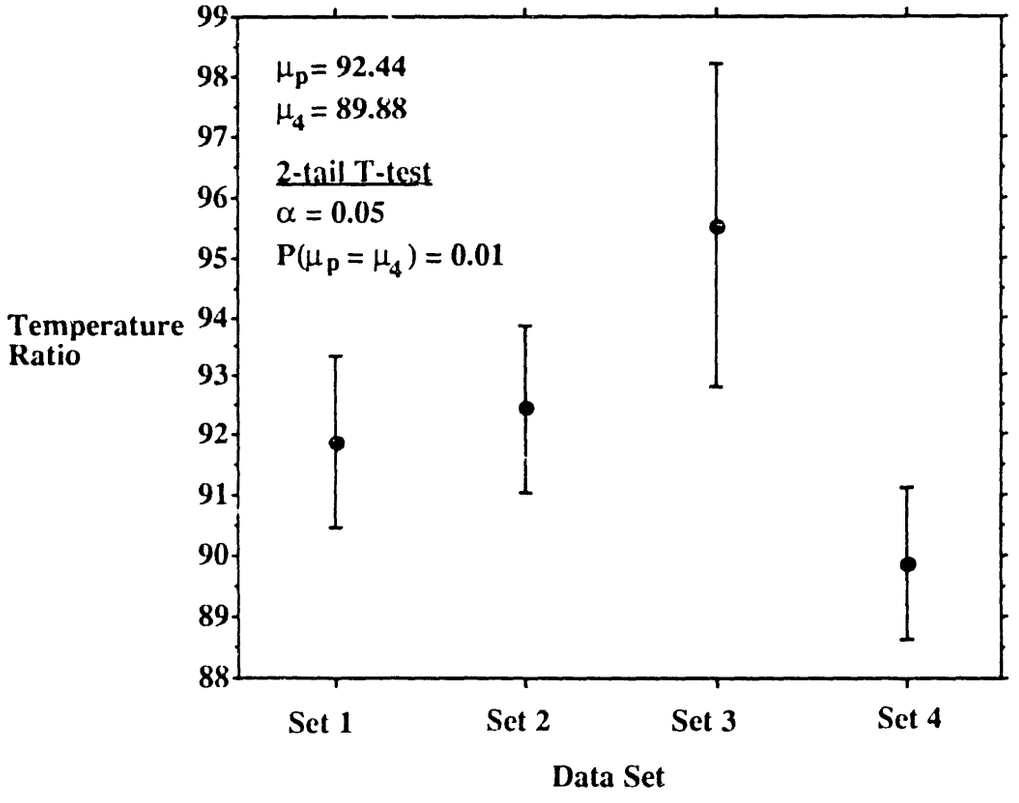

Figure 4. Comparison of the mean and standard deviations of 4 data sets taken from the same specimen, sputtered Si on Si, showing a low probability of set 4 belonging to the entire population.

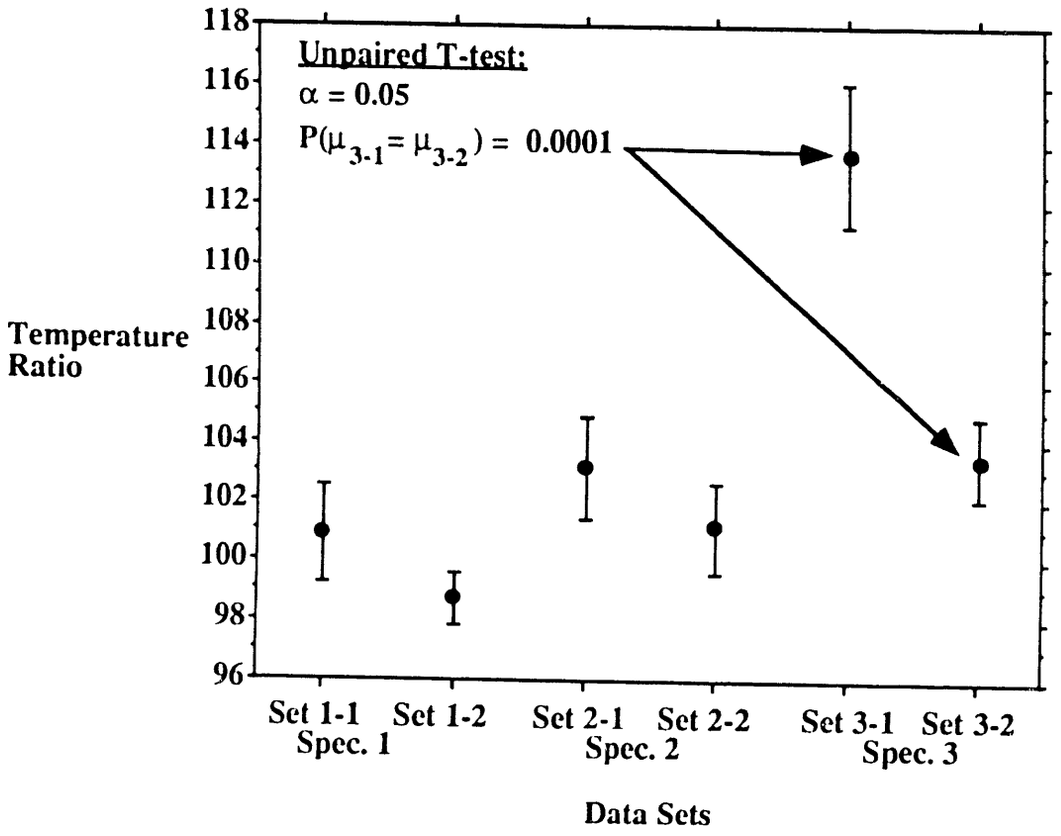

Figure 5. Mean and standard deviation of two separate data sets for each of three specimens (three thicknesses) of sputtered Si_3N_4 on Si showing lack of correlation for the two sets taken on the thickest specimen, specimen 3. Other data sets are well correlated.

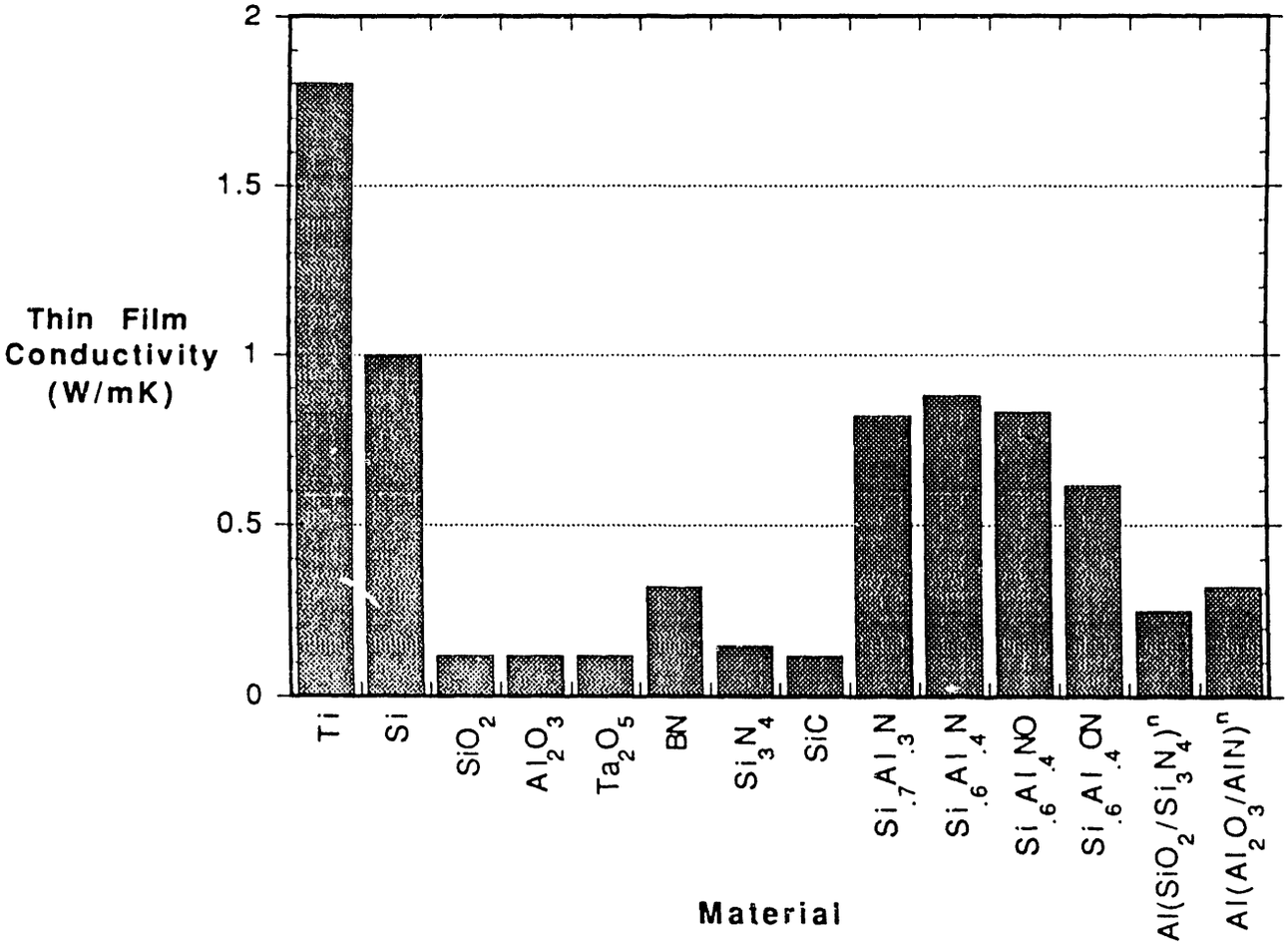

Figure 6. Measured thin film thermal conductivities of various sputtered optical films and multi-layered stacks.

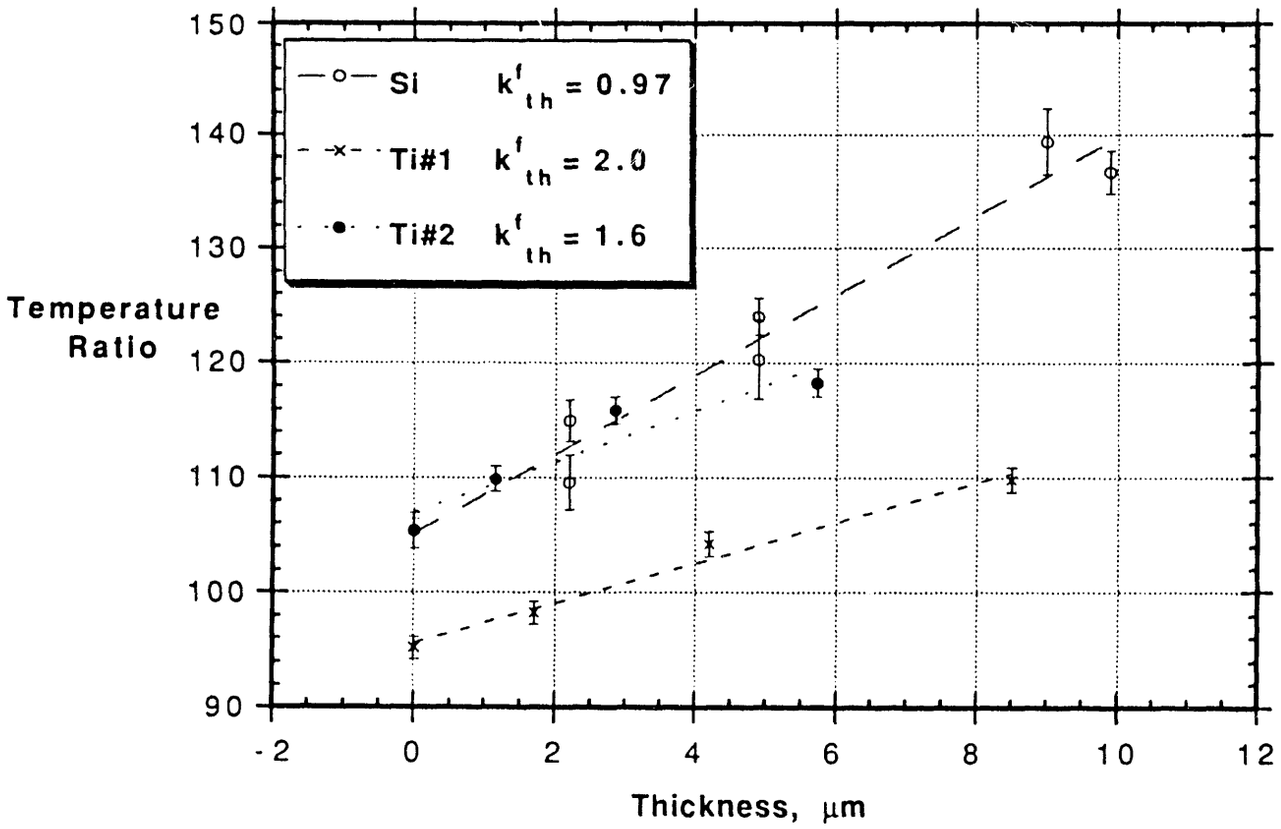

Figure 7. Measured thermal conductivities of sputtered Ti and Si films (in W/mK).

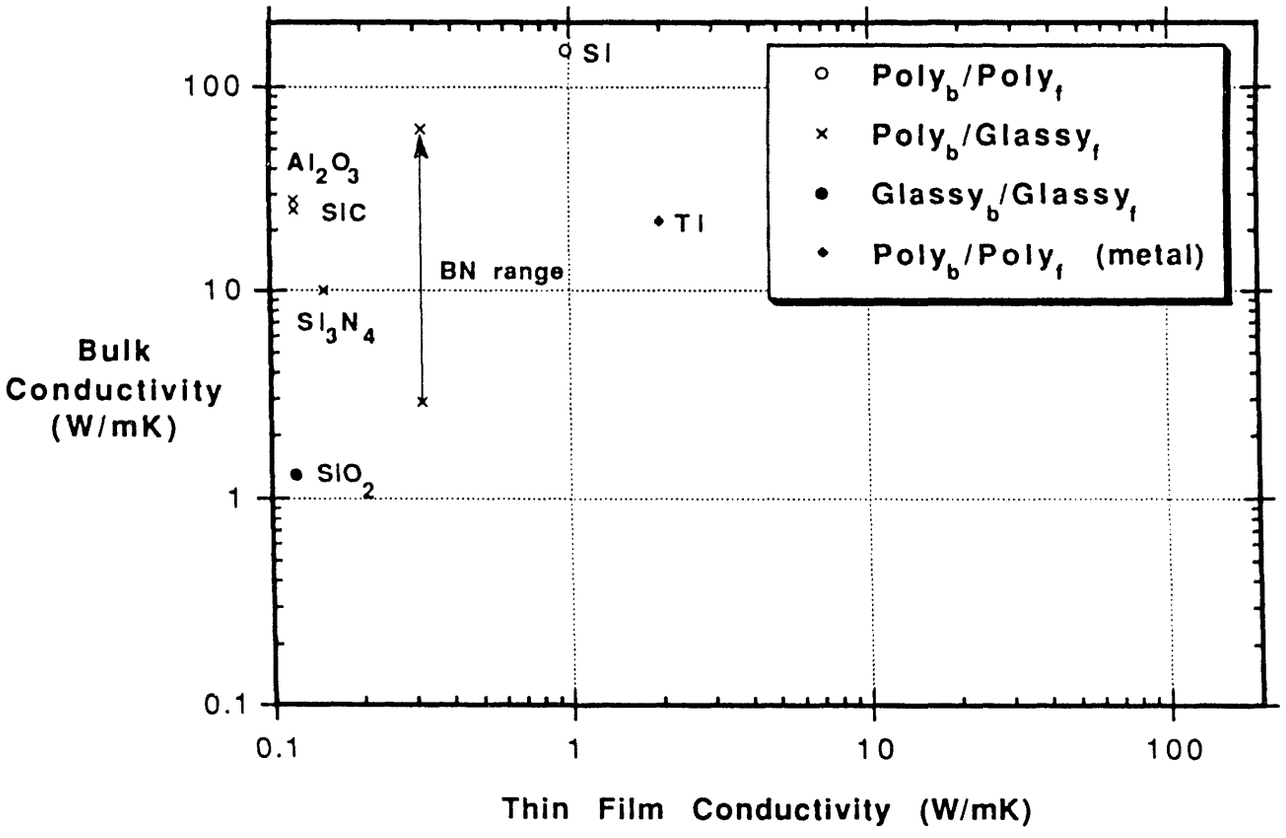

Figure 8. Comparison of Handbook bulk thermal conductivities with measured thin film conductivities. Data segregated based on bulk and film structure, polycrystalline or glassy.

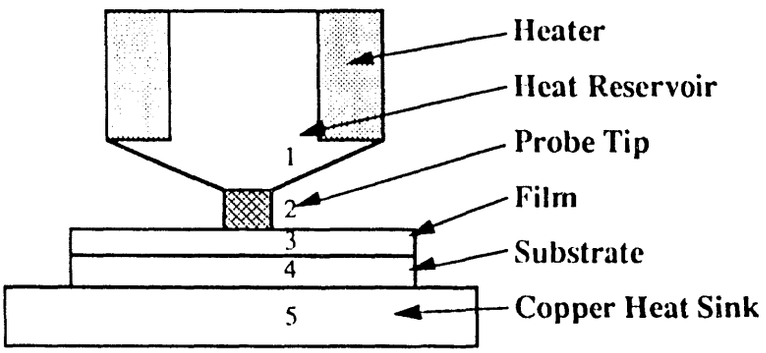

Figure A1. Schematic of probe tip region of thermal conductivity apparatus.

END

DATE
FILMED
01/31/92